



CHORUS

This is the accepted manuscript made available via CHORUS. The article has been published as:

Imaging and Control of Surface Magnetization Domains in a Magnetoelectric Antiferromagnet

Ning Wu, Xi He, Aleksander L. Wysocki, Uday Lanke, Takashi Komesu, Kirill D. Belashchenko, Christian Binek, and Peter A. Dowben

Phys. Rev. Lett. **106**, 087202 — Published 23 February 2011

DOI: [10.1103/PhysRevLett.106.087202](https://doi.org/10.1103/PhysRevLett.106.087202)

Imaging and control of surface magnetization domains in a magnetoelectric antiferromagnet

Ning Wu,¹ Xi He,¹ Aleksander L. Wysocki,¹ Uday Lanke,² Takashi Komesu,¹ Kirill D. Belashchenko,¹ Christian Binek,¹ and Peter A. Dowben¹

¹*Department of Physics and Astronomy and Nebraska Center for Materials and Nanoscience, University of Nebraska-Lincoln, Lincoln, Nebraska 68588, USA*

²*Canadian Light Source Inc., University of Saskatchewan, 101 Perimeter Road, Saskatoon, Saskatchewan, Canada S7N 0X4*

We report the direct observation of surface magnetization domains of the magneto-electric Cr_2O_3 using photoemission electron microscopy with magnetic circular dichroism contrast and magnetic force microscopy. The domain pattern is strongly affected by the applied electric field conditions. Zero-field-cooling results in an equal representation of the two domain types, while electric-field-cooling selects one dominant domain type. These observations confirm the existence of surface magnetization, required by symmetry in magnetoelectric antiferromagnets.

PACS numbers: 75.85.+t, 75.70.Rf, 75.70.Kw, 78.70.Dm, 78.20.Ls

Magnetoelectric antiferromagnets [1] have an equilibrium boundary magnetization, which is coupled to the bulk antiferromagnetic order parameter [2–4]. Boundary (surface) magnetization was detected at the $\text{Cr}_2\text{O}_3(0001)$ surface using spin-polarized photoemission spectroscopy as well as through exchange bias in a proximate ferromagnetic film [2]. Degenerate time-reversed domain states with opposite boundary magnetization can be switched magnetoelectrically [5], enabling electrically switchable exchange bias [2]. This approach offers a promising new route to voltage-controlled spintronic devices, such as non-volatile magnetoelectric memory [6, 7], which may be viewed as an alternative to other approaches based on multiferroics [8–10].

Until now, only macroscopically averaged signatures of the equilibrium boundary magnetization have been observed [2]. Here we report spatially resolved observations of the electrically controlled magnetization domain structure at the surface of magnetoelectric $\text{Cr}_2\text{O}_3(0001)$ films using magnetic force microscopy (MFM) and photoemission electron microscopy (PEEM) combined with X-ray magnetic circular dichroism (XMCD) contrast.

Cr_2O_3 thin films were grown on single crystal $\text{Al}_2\text{O}_3(0001)$ substrates by molecular beam epitaxy at a base pressure of 4×10^{-10} mbar. Metallic Cr was evaporated and transformed into the stable Cr_2O_3 oxide using an oxygen partial pressure of 2.6×10^{-6} mbar. The resulting 127 nm thick Cr_2O_3 films have (0001) orientation, as shown in Fig. 1a.

The atomic and magnetic force microscopy (AFM and MFM) experiments were performed in the tapping/lift mode. In the lift mode the tip was placed 20 nm above the surface. In addition to the AFM image taken at $T = 296.0$ K (Fig. 1b), other virtually identical AFM images were taken at 299.6, 304.9, and 319.3 K to complement the MFM images shown in Fig. 2. Fig. 1c reveals a root-mean-square roughness of 0.17 nm typical for large portions of the surface. These smooth regions are inter-

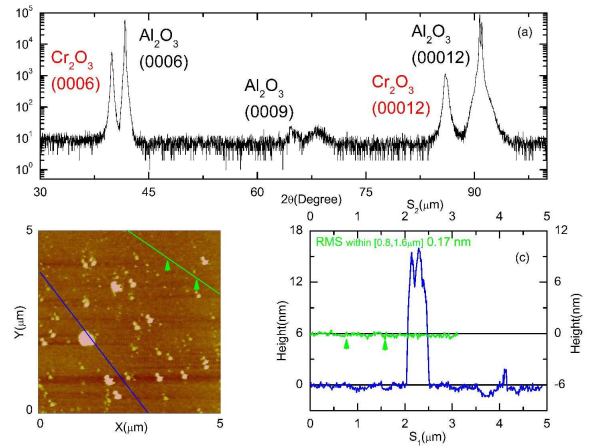


FIG. 1: (a) X-ray diffraction pattern showing the $\text{Cr}_2\text{O}_3(0006)$ and (00012) peaks. The Al_2O_3 substrate contributes the (0006) , (00012) diffraction features and a weak structure-factor-forbidden (0009) peak. (b) Topographic AFM image of the $\text{Cr}_2\text{O}_3(0001)$ film surface. (c) Height profiles along the blue and green lines of panel (b) parameterized by S_1 and S_2 . Root-mean-square roughness of 0.17 nm is estimated in the region of S_1 from 0.8 to 1.6 μm .

rupted by structural defects with heights of up to 16 nm.

The MFM done after zero-field cooling to 296 K (Fig. 2a) reveals magnetic contrast between the surface magnetization domains (red and green), which reflect the underlying antiferromagnetic domains and are equiprobable, as expected from their energetic degeneracy. The contrast fades out while going across the bulk Néel temperature $T_N = 308$ K, and by 319.3 K it disappears completely (Fig. 2d), which proves its magnetic origin. The magnetic domain size is about 2–3 μm . The MFM contrast is expectedly weak, because the measured magnetic field is produced by just a thin magnetized layer at the surface. In addition, close to T_N the antiferromagnetic order

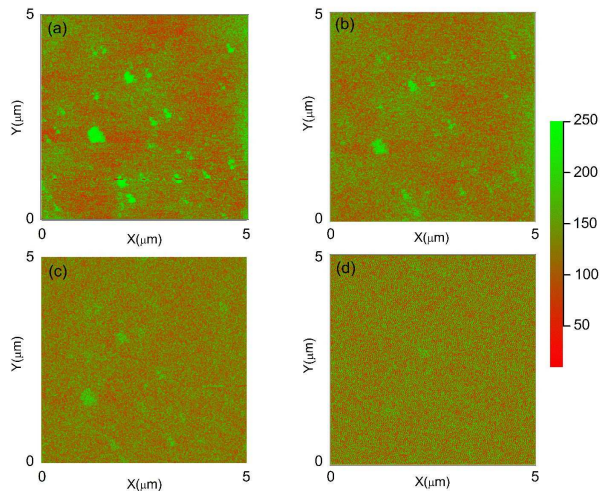


FIG. 2: MFM images for the same scanning area as in Fig. 1b. (a) 296.0 K. (b) 299.6 K. (c) 304.9 K. (d) 319.3 K.

parameter and the surface magnetization are small [2].

Comparison of Figs. 1b and 2a shows that narrow columnar defects also provide magnetic contrast disappearing above T_N . The magnetization of all these defects in the same direction; this feature is likely induced by the tip. At each scanning position the tip is initially brought into contact with the surface and then lifted up to a height of 20 nm. During contact the columnar defects, being magnetically decoupled, can become magnetized by the tip. The finer contrast at the scale of 100 nm or smaller, which persists above T_N , is probably noise.

The XMCD-PEEM contrast is sensitive to uncompensated spins within the sampling depth of about 2 nm [11]. The XMCD-PEEM combination has been used to study the exchange bias on systems like Co/LaFeO₃ [12]. For a conventional antiferromagnet the XMCD contrast vanishes [11, 13]. Some contrast due to bulk magnetochiral dichroism may be expected for Cr₂O₃ [14], but this effect is very small compared to the XMCD signal recorded here, and it is also suppressed by the XMCD PEEM geometry. Unlike the previously measured Cr XMCD signal for the Cr₂O₃/Pt/Co heterostructure (where the domain structure could not be clearly imaged) [15], our measurements were done for the free surface of Cr₂O₃ and were therefore not influenced by a proximate ferromagnet.

X-ray PEEM studies were carried out at the Spectromicroscopy beamline at the Canadian Light Source [16], capable of producing linearly and circularly polarized photons from 130 eV to 2500 eV. The elliptically polarized APPLE II type undulator delivers close to 100% right or left circularly-polarized light, although the beamline optics result in up to 4% polarization attenuation at the Cr $2p$ edges (i. e. at 550-880 eV). The incident light on the sample remains $95 \pm 2\%$ circularly polarized. The incident intensity remained the same when the polariza-

tion was changed from left to right and back. Spatial resolution of the Elmitec GmbH PEEM microscope is better than 30 nm for an ideal flat sample.

The XMCD intensity is proportional to the projection of the magnetization on the X-ray polarization direction. PEEM images obtained with left and right circularly polarized light, incident at a 74° angle from the surface normal at a photon energy of 578.3 eV, were used to generate the images shown in Fig. 3. When magnetization is aligned parallel (antiparallel) to the photon angular momentum, there is a maximum (minimum) intensity in the absorption yield spectra. This is denoted in the inset to Fig. 3. The PEEM images taken with left and right circularly polarized light show opposite contrast.

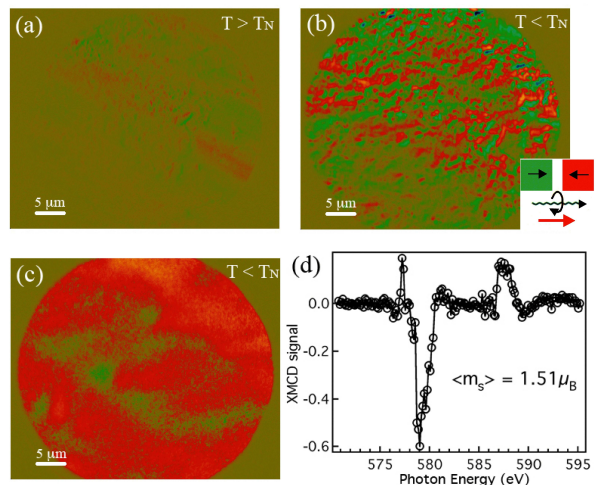


FIG. 3: (a-c) Cr₂O₃ (0001) film imaged by XMCD-PEEM at the Cr L-edge. (a) No contrast at 584 K. (b) Multi-domain state after zero-field cooling. (c) Nearly single-domain state at 223 K after magnetoelectric field cooling. (d) XMCD spectrum recorded from within one domain. The inset indicates the qualitative spin polarization in the image with respect to positively circularly polarized incident light.

Fig. 3a shows the reference PEEM-XMCD image (Cr L₃ edge) recorded at 584 K (well above T_N), where no magnetic domains are seen. The residual contrast is due to beam effects and optical imperfections, as expected for a surface far from perfectly flat. Conversely, clear contrast is seen at 223 K in the multi-domain state after zero-field cooling (Fig. 3b), giving a direct image of surface magnetic domains. The characteristic domain size is 3-5 μm similar to that observed in MFM (Fig. 2a). In Fig. 3b the ratio of areas with positive and negative contrast is 56:44, which is statistically consistent with the absence of a preferential domain orientation expected for degenerate domains.

Fig. 3c displays the XMCD image recorded after magnetoelectric field cooling across T_N in a 13.3 kV/mm electric field applied close to the surface normal and in the presence of the Earth's magnetic field. Magnetoelec-

tric field cooling lifts the degeneracy of the 180° antiferromagnetic domains, thereby stabilizing one of them [1, 2, 6, 17]. This results in a strong preponderance of the stabilized domain variant and produces domains of a much larger size. In Fig. 3c the area ratio of the two domain variants is 96:4. In the present case, the product of electric and magnetic fields is greater compared to our earlier study, where spin-polarized photoemission measured 80% spin polarization in the region of the Cr_2O_3 surface [2]. The selection of one magnetization orientation observed in Fig. 3c demonstrates electric control of surface magnetic domains.

The microscopic surface magnetic domain pattern revealed by MFM (Fig. 2) and XMCD PEEM (Fig. 3) is attributable to the symmetry of magnetoelectric antiferromagnets [3, 4]. In a generic antiferromagnet such domains could only appear if the surface was close to atomically flat, with domains coinciding with atomically flat steps; otherwise the surface magnetization is destroyed by roughness. Although our film samples have a rather small nominal roughness, it is highly unlikely that micron-scale regions of the surface are atomically flat; in particular, no atomic steps are seen by AFM. In addition, some areas of the sample exhibit height variations of a few nanometers over a micron lateral scale (note the deep horizontal trough in the lower portion of Fig. 1b). These areas do not affect the magnetic domain pattern seen in the MFM images, which proves that this contrast does not require atomically flat regions.

The XMCD spectrum recorded at a single $1\ \mu\text{m}^2$ spot is shown in Fig. 3d. Using standard sum rules [18], we deduce the lower bound for the local spin magnetic moment of $1.51\ \mu_B$ per Cr atom, which is likely underestimated due to the possible misalignment of the Cr^{3+} spin moments and the photon polarization direction. This large value rules out the bulk magnetoelectric effect as the source of the XMCD contrast. On the other hand, since XMCD-PEEM is not completely surface-sensitive, the apparent spin magnetic moment is reduced by the signal from the antiferromagnetic bulk of Cr_2O_3 ; it may also be affected by the approximations in applying the spin sum rules to the electron yield from Cr^{3+} .

The net spin polarization seen in XMCD-PEEM cannot always be attributed to the surface. However, comparison of the XMCD spectrum with spin-polarized inverse photoemission (SPIPES), which is almost entirely surface-sensitive [19, 20], and first-principles calculations suggest that the XMCD-PEEM contrast observed here is predominantly a surface effect. Fig. 4a shows X-ray absorption at the Cr L_3 edge taken by left and right circularly-polarized light from within one magnetic domain (red area of Fig. 3c). The XMCD absorption reflects electronic transitions from the $2p_{3/2}$ core level to the unoccupied majority-spin (minority-spin) $3d$ states induced predominantly (but not exclusively) by photons with positive (negative) helicity [20]. The main peak of

the L_3 edge is at a photon energy of 579 eV. Given that the X-ray photoemission spectroscopy gives the Cr $2p_{3/2}$ binding energy of 576.8 eV [21], this places the unoccupied minority peak at about 3 eV above the Fermi level.

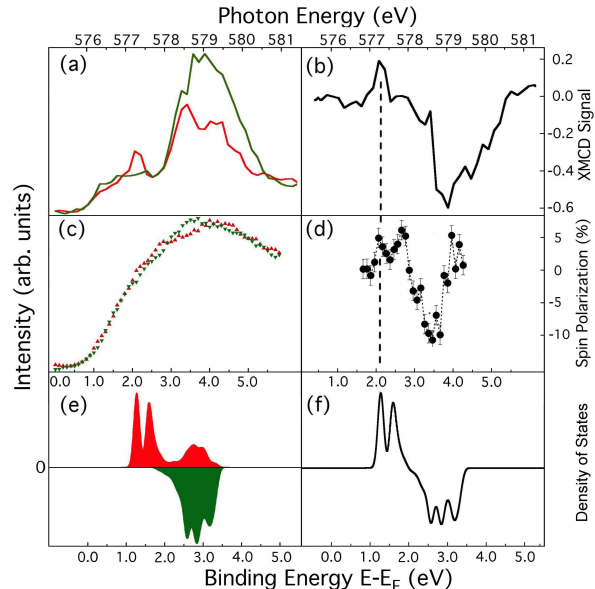


FIG. 4: (a) XMCD absorption at the Cr L_3 edge taken by left (red) and right (green) circularly-polarized light from a $1\ \mu\text{m}^2$ spot in the red area of Fig. 3c. (b) XMCD signal derived from (a). (c) Unoccupied spin up states and spin down states taken by SPIPES at 300 K. (d) Spin polarization of unoccupied states derived from (c). (e) Calculated majority-spin (red) and minority-spin (green) DOS for the Cr_2O_3 surface. The energy is referenced from the surface valence band maximum. (f) Difference of the majority-spin and minority-spin DOS from (e). The energy scales are the same in all panels, but the first majority-spin peaks are aligned (dashed lines) to remove the uncontrollable energy shifts due to different final state effects and other uncertainties.

Fig. 4c shows the results of SPIPES measurement for a Cr_2O_3 overlayer thin film, performed as detailed elsewhere [22]. The spin polarization shown in Fig. 4d varies between 5% to -10% . This small value may be due to the measurement geometry, which is sensitive to the net in-plane spin polarization, while the surface spins may tend to be oriented out-of-plane. Because SPIPES and XMCD are final-state spectroscopies where the final state effects [20, 23] induce unknown shifts in the apparent binding energies (or photon energy), we have lined up the spectra in Fig. 4 according to the first significant feature in the unoccupied density of states (DOS). Comparison of panels (b) and (d) of Fig. 4 shows that there is a qualitative correspondence between XMCD and SPIPES data, although the selection rules do differ and perfect agreement is not expected [19, 20]. In particular, both measurements show that at about 3 eV above the Fermi level the minority-spin density of states (DOS) is higher than the majority-spin DOS.

Further, we performed first-principles calculations for the Cr_2O_3 (0001) surface using the supercell method. We considered a symmetric slab consisting of eight atomic layers of O and 16 atomic layers of Cr stacked along the (0001) direction and separated from its image by 1.5 nm of vacuum. The lateral dimensions of the supercell were fixed to the bulk values [24] and all ions were allowed to relax. We employed the spherically symmetric LDA+U [25] and projector augmented wave method [26] as implemented in the VASP code [27, 28]. We used $U = 4$ eV and $J = 0.58$ eV as for bulk Cr_2O_3 [24] and a plane-wave energy cutoff of 520 eV. For the $\sqrt{3} \times \sqrt{3}$ surface supercell discussed below we used a $3 \times 3 \times 1$ k -point mesh for relaxation and a $6 \times 6 \times 1$ mesh for the DOS calculation.

We considered the stoichiometric surface terminated with a single layer of Cr, which is known to be stable [29]. We found two competing surface Cr sites, one (site A) similar to the site resulting from termination of the bulk crystal (site 2 in Ref. [29]) and the interstitial site below the oxygen subsurface layer [30] (site B). We established that the ground state structure has $\sqrt{3} \times \sqrt{3}$ ordering with two surface Cr atoms at A sites and one surface Cr atom at a B site. The electronic structure is calculated for this ground state, although we note that at the experimental temperatures the A-B site disorder can affect the surface electronic structure. (More details will be published elsewhere.) The unoccupied part of the spin-resolved partial DOS for these three surface Cr sites is shown in Fig. 4e. (The energy zero is at the highest occupied level of the slab, which is about 1 eV above the bulk valence band maximum judged by the central Cr layers.) Two narrow majority-spin peaks at 1.3 eV and 1.6 eV come from the two inequivalent A sites. These peaks are shifted with respect to each other due to different electrostatic potentials at these sites. The first and part of the second of these peaks lie inside the bulk band gap. The broad majority-spin feature at about 2.8 eV arises from the B site. Minority-spin peaks at 2.6 eV and 2.8 eV come from the t_{2g} -derived states of the two A sites, while the peak at 3.2 eV originates from the e_g -derived states of these A sites. The minority-spin states of the B site strongly hybridize with the neighboring oxygen atoms and form a broad peak in the same energy region.

The calculated DOS (Fig. 4d) shows that there is a fairly narrow majority-spin surface band, which forms the conduction band minimum. This band is therefore expected to provide the leading edge for electronic transitions observed in XMCD and SPIPES spectra, which is consistent with Fig. 4d and 4f. The exchange splitting of the conduction band survives at the surface. These features provide further support of the dominant surface origin of the magnetic contrast observed in XMCD-PEEM and MFM.

In summary, surface magnetization domains of the magnetoelectric Cr_2O_3 surface were imaged by MFM and XMCD-PEEM, and their magnetoelectric control

was demonstrated. These results confirm and extend the results of macroscopically averaged observations of the boundary magnetization of Cr_2O_3 [2].

This work was supported by NSF through DMR-0547887, the Nebraska MRSEC (DMR-0820521), and by the NSF/SRC-NRI supplement to the Nebraska MRSEC. K.B. is supported by a Cottrell Scholar Award from the Research Corporation. The PEEM work was performed at the Canadian Light Source, which is supported by the NSERC, NRC Canada.

-
- [1] M. Fiebig, *J. Phys. D* **38**, R123 (2005).
- [2] Xi He *et al.*, *Nature Mater.* **9**, 579 (2010).
- [3] A. F. Andreev, *JETP Lett.* **63**, 724 (1996).
- [4] K. D. Belashchenko, *Phys. Rev. Lett.* **105**, 147204 (2010).
- [5] T. J. Martin and J. C. Anderson, *IEEE Trans. Magn.* **2**, 446 (1966).
- [6] C. Binek and B. Doudin, *J. Phys.: Condens. Matter* **17**, L39 (2005).
- [7] M. Bibes and A. Barthélémy, *Nature Mater.* **7**, 425 (2008).
- [8] W. Eerenstein, N. D. Mathur and J. F. Scott, *Nature* **442**, 759 (2006).
- [9] R. Ramesh and N. A. Spaldin, *Nature Mater.* **6**, 21 (2007).
- [10] S.-W. Cheong and M. Mostovoy, *Nature Mater.* **6**, 13 (2007).
- [11] J. Stöhr *et al.*, *Surf. Rev. Lett.* **5**, 1297 (1998).
- [12] F. Nolting *et al.*, *Nature* **405**, 767 (2000).
- [13] H. Ade and H. Stoll, *Nature Mater.* **8**, 281 (2009).
- [14] J. Goulon *et al.*, *Phys. Rev. Lett.* **88**, 237401 (2002).
- [15] P. Borisov *et al.*, *J. Magn. Magn. Mater.* **310**, 2313 (2007).
- [16] K. V. Kaznatcheev *et al.*, *Nuc. Instr. Methods A* **582**, 96 (2007).
- [17] P. Borisov *et al.*, *Phys. Rev. Lett.* **94**, 117203 (2005).
- [18] J. Stöhr and H. C. Siegmann, *Solid State Sciences, Magnetism (From Fundamentals to Nanoscale Dynamics)*, Vol. 152 (Springer-Verlag, Berlin Heidelberg, 2006).
- [19] N. V. Smith, *Prog. Surf. Sci.* **51**, 1227 (1988).
- [20] C. N. Borca, T. Komesu, and P. A. Dowben, *J. Electron Spectrosc. Rel. Phenom.* **122**, 259 (2002).
- [21] R. Cheng *et al.*, *Appl. Phys. Lett.* **79**, 3122 (2001).
- [22] R. Cheng *et al.*, *Phys. Lett. A* **302**, 211 (2002).
- [23] J. E. Ortega *et al.*, *Solid State Commun.* **91**, 807 (1994).
- [24] S.-Q. Shi, A. L. Wysocki, and K. D. Belashchenko, *Phys. Rev. B* **79** 104404 (2009).
- [25] A. I. Liechtenstein, V. I. Anisimov, and J. Zaanen, *Phys. Rev. B* **52**, R5467 (1995).
- [26] P. E. Blöchl, O. Jepsen, and O. K. Andersen, *Phys. Rev. B* **49**, 16223 (1994).
- [27] G. Kresse and J. Hafner, *Phys. Rev. B* **48**, 13115 (1993).
- [28] G. Kresse and J. Furthmüller, *Phys. Rev. B* **54**, 11169 (1996).
- [29] M. Bender *et al.*, *J. Phys.: Condens. Matter* **7**, 5289 (1995).
- [30] Th. Gloege *et al.*, *Surf. Sci. Lett.* **441**, L917 (1999).